BULLETIN OF THE POLISH ACADEMY OF SCIENCES
TECHNICAL SCIENCES, Vol. 71(4), 2023, Article number: e146237
DOI: 10.24425/bpasts.2023.146237



# Effects of ageing heat treatment temperature on the properties of DMLS additive manufactured 17-4PH steel

**Aleksander ŚWIETLICKI[1]*, Mariusz WALCZAK[1], Mirosław SZALA[1], Marcin TUREK[2] and Dariusz CHOCYK[3]**

[1] Department of Materials Engineering, Faculty of Mechanical Engineering, Lublin University of Technology, Nadbystrzycka 36, 20-618 Lublin, Poland

[2] Institute of Physics, Maria Curie-Sklodowska University in Lublin, pl. M. Curie-Sklodowskiej 1, 20-031 Lublin, Poland

[3] Department of Applied Physics, Faculty of Mechanical Engineering, Lublin University of Technology, Nadbystrzycka 36, 20-618 Lublin, Poland

**Abstract.** Additive manufacturing (AM) is a modern, innovative manufacturing method that enables the production of fully dense products with high mechanical properties and complex shapes that are often impossible to obtain by traditional methods. The 17-4PH grade steel is often applied where high mechanical performance is required. 17-4PH, or AISI 630, is intended for precipitation hardening, an operation that combines solution and ageing treatments and is used to significantly change the microstructure of the steel and enhance its mechanical properties. This study investigates the effect of precipitation hardening on the properties of 17-4PH steel. To examine microstructure and morphology, metallographic tests were performed together with phase composition and chemical composition analyses. Mechanical parameters were determined via Vickers hardness testing and the Oliver-Pharr method. Samples were fabricated using direct metal laser sintering (DMLS), which is one of the powder bed fusion methods. The use of a constant solution treatment temperature of 1040°C and different ageing temperatures made it possible to evaluate the effects of ageing temperature on the mechanical properties and microstructure of 17-4PH. The presence of face-centered cubic FCC $\gamma$-austenite and body-centerd cubic BCC $\alpha$-martensite structures were detected. The tests revealed that – similarly to the wrought material – the highest hardness of $382 \pm 10.3$ $HV_{0.2}$ was obtained after ageing at 450°C. The nanoindentation test showed the same H/E ratio for the sample after fabrication and after solution treatment at 0.016769, but this value increased after ageing to 127–157.5%. The sample aged at 450°C was characterized by the highest H/E ratio of 0.026367, which indicates the highest wear resistance of this material under employed treatment conditions. In general, the sample treated at 450°C showed the best performance out of all tested samples, proving to have the smallest grain size as well as high Vickers and nanoindentation hardness. On the other hand, the use of solution treatment led to reduced hardness and improved workability of the AM material.

**Key words:** 17-4PH steel; precipitation hardening; additive manufacturing; heat treatment; nanohardness.

## 1. INTRODUCTION

The 17-4PH grade of steel has highly desirable properties due to its high mechanical strength and hardness at an elevated temperature (300°C) combined with high corrosion resistance, good weldability [1], and reasonable workability. Nevertheless, its mechanical properties can be further improved by the use of proper heat treatment, primarily precipitation hardening. This study investigates the effect of manufacturing conditions on the microstructure and properties of DMLS-produced 17-4PH specimens for variable temperature and heat treatment time.

Owing to its properties, the 17-4PH steel grade is widely used in the aerospace industry [2]. Another use for this steel grade is in nuclear power plants [3]. Bolts and exhaust fasteners are examples of applications for 17-4PH steel in the automotive industry [4]. In medicine, 17-4PH steel is used for orthopaedics [5], dental applications, and surgical forceps [6]. Given that medical applications often require complex shapes, especially for implants and surgical instruments, a modern approach to this problem is the use of materials produced by additive technologies [7].

Recently, there has been progress in the development of additive manufacturing (AM) technologies. AM is the transformation of a digital CAD model into a real part through layer-by-layer creation [8]. AM is used to manufacture objects from metals, ceramics, composites, polymers, and organic structures [9]. 17-4PH is one of the most widely used steels for precipitation hardening (PH), especially in ingot metallurgy, and one of the most widely used powders in the metal injection moulding industry [10]. The application of the AM technology combined with 17-4PH steel properties makes it possible to achieve a high quality of manufactured parts and meet the requirements of complex shapes for the automotive [3], aerospace [4], and injection moulding industries. The main advantages of AM over conventional manufacturing methods include: high automation of the manufacturing process even when compared to CNC ma-

*e-mail: aleksander.swietlicki@pollub.edu.pl

Manuscript submitted 2023-02-22, revised 2023-05-05, initially accepted for publication 2023-06-01, published in August 2023.

chining, the lower single unit cost in small batches, and low material loss due to machining [11].

On the other hand, components produced by additive technologies are not free from defects such as unmelted particles, anisotropic properties, and porosities due to pool weld collapse [12]. Residual stresses and delamination during manufacturing lead to reduced repeatability and reliability [13]. AM-fabricated components often require additional processes to increase their mechanical properties and some of these disadvantages can be eliminated. Therefore, processes such as heat treatment and shot peening may be utilized for direct metal laser sintering (DMLS) components [14].

AM can be divided into three groups depending on the powder bed, powder feed, and wire feed methods [11]. DMLS technology is a powder bed fusion (PBF) method that is often used for additive manufacturing. As the PBF technology, DMLS allows a wide range of materials to be manufactured at relatively low cost in low series production [11]. The application of the DMLS technique makes it possible to obtain high repeatability of strength properties of produced elements, and the density of the elements produced thereby is about 95% [15]. It is also important that the DMLS method does not require the use of a flux or polymer binder, thus the firing and infiltration steps can be avoided. Nonetheless, it may be problematic to support some structures during printing [16].

If produced by traditional methods, 17-4PH is usually martensitic steel with a small amount of residual austenite and/or ferrite [10, 17, 18]. As a result of transformations associated with the employed AM method and the composition of the 3 phases after AM, there may occur changes in the proportions of individual components. This is due to, among other things, the thermal history of a component after additive manufacturing, i.e. repeated heating and cooling of a single piece of material that used to be powder grain. Nevertheless, the state of the material after heat treatment also depends on the composition of the powder and the gases used for manufacturing. The final proportion of individual phases and obtained properties also depend on the employed heat treatment and, thus, the time and temperature of solutionizing and ageing treatments.

Considering the properties of 17-4PH as well as the advantages of the direct metal laser sintering (DMLS) technique and the opportunities offered by precipitation hardening, it is reasonable that these methods be merged to produce a part that combines high mechanical strength, good ductility, and high corrosion resistance with complex shape.

17-4PH is martensitic steel, and precipitation hardening occurs by precipitation of highly dispersed copper particles in the martensite matrix [19]. Precipitation hardening has a beneficial effect on the properties of 17-4PH steel by removing anisotropy and making the structure homogenised. For 17-4PH steel after 3D printing, there is an increase in the amount of residual austenite in the structure, in contrast to the same alloy produced by casting where the structure is almost entirely martensitic. When ageing 17-4PH steel after additive manufacturing, $M_{23}C_6$, and $M_7C_3$ type carbides are released. A uniform distribution of austenite stabilizing elements can also lead to a lower MS temperature during ageing conducted above 480°C. At the same time, the structure in the range 480–620°C changes from copper-rich coherent BCC to non-coherent FCC, which leads to reduced hardness and increased ductility [13]. On the other hand, the segregation of austenite stabilizing elements may lead to crack formation [20]. S. Cheruvathur *et al*. [21] found a dendritic cellular structure and almost equal proportions of martensite and austenite in the as-built structure, while the structure of the wrought material was almost entirely martensitic. Although the annealing of as-built parts at 650°C for 1h was not sufficient to improve their properties, particularly good results were obtained after homogenisation annealing at 1150°. The application of this treatment allowed the dendritic solidification microstructure to be broken down, micro-segregation to be alleviated, as well as 90% martensite and 10% austenite to be obtained.

Studies have shown that 17-4PH steel does not exhibit cytotoxicity, metal release, or weight loss [22]. It is resistant to stress corrosion cracking. The properties of this steel grade have been widely described. Singh *et al*. [23] investigated the possibility of using DMLS-produced 17-4PH steel for intramedullary (IM) pins. Many properties depend on fabrication parameters such as scanning strategy, layer thickness, or building direction [24]. Guennouni *et al*. [25] compared the properties of 17-4PH steel produced by casting with that produced by laser beam melting. The samples were subjected to the same heat treatment. No major differences were observed in the chemical composition and during a microscopic examination; however, more porosity and carbides were visible in the samples after additive manufacturing. There was also a significant increase in the amount of both secondary and residual austenite for the additive manufactured samples at 12.6% and 0.8% respectively for the conventional samples. Despite this significant increase in the amount of austenite, the tensile properties remained at a similar level. That being said, some reduction in ductility was noted.

Siddiqui *et al.* [26] presented the mechanical material characteristics of 17-4PH steel produced by the DMLS technique. GP1 powder and an EOSINT M280 printer were used. Tests were carried out on samples produced in the *x*- and *y*-axes. It was noted that the tensile tests showed slightly anisotropic properties for the *x*-axis and *y*-axis fabrications. Low-cycle fatigue tests showed isotropic behaviour for the *x*- and *y*-axis fabrications. The anisotropic properties may be due to defects in microstructure occurring during fabrication. It was also suggested that the cyclic hardening could be attributed to the strain-induced metastable phase transformation of austenite to martensite. Gorunov *et al*. [27] found that the cyclic resistance of 17-4PH steel produced by DMLS increased for the 0.5, 1.0, and 2.5 mm notched specimens compared to the unnotched specimen. It was also found that the creep strength could be reduced due to internal discontinuities, geometric notching, or roughness. The unpredictability of complex-shape structures fabricated via DMLS was suggested, as heat concentration can affect heterogeneity and stress concentration during sintering.

The use of heat treatment yields good results for metallic materials produced by additive manufacturing. S. Razavi *et al*. [28] conducted a study using artificial neural networks and a genetic

algorithm to predict the effect of precipitation hardening on 17-4PH steel. A good model was able to predict the hardness as a function of temperature and time of precipitation hardening. It was also emphasized that the solutionizing temperature should be in a range of about 1050°C, as indicated by the Fe-C-Cu diagram. An insufficient temperature can lead to a decrease in austenite stability and the separation of copper and alpha phases. If it is too high, this can lead to grain growth and, consequently, to a decline in mechanical properties. By increasing compressive residual stresses, the fatigue and tensile properties can also be improved.

Wear is an important aspect of all engineering material applications. Wear and tear lead to shorter product life and is undesirable for implants that are problematic or completely impossible to replace [29].

Researchers have attempted to describe the behaviour of 17-4PH, yet the characteristics of AM-fabricated structures differ significantly. There are very few studies on this steel grade after DMLS printing and, especially, after heat treatment. Most studies focus on global material properties such as tensile strength or hardness tested by Vickers and Rockwell methods, but at the nanoscale, there are no studies providing hardness or elastic modulus results. In particular, one can see a gap in studies devoted to describing the anti-wear properties of 17-4PH steel after AM. A review of the literature shows that the problems that are worth considering include phase composition, temperatures, and processing time. Most of the current research on AM 17-4PH steel is conducted in the H900 to H1150M treatment range, which means ageing at temperatures from 482°C to 760°C for 1 h, 4 h, or 2+4 h. The objective of this study is to determine the most promising parameters of the precipitation hardening process by applying variable ageing temperature, as well as to investigate their influence on the final microstructure and mechanical properties of this steel grade. A novelty of this study is that it employs the Oliver–Pharr method after heat treatment to provide results of the H/E ratio and, at the same time, to estimate the resistance of the material to erosive wear. This study aimed to determine optimum conditions for obtaining the most promising operational parameters, such as wear resistance, hardness, and elasticity modulus for AM 17-4PH steel.

## 2. EXPERIMENTAL PROCEDURE

The test material was 17-4PH grade stainless steel (also designated as AISI 630, X5CrNiCuNb16-4, or 1.4542) that was produced by DMLS powder sintering. The sintered material was stainless steel GP1 powder, which, according to the manufacturer, is characterised as a 17-4PH, separable-reinforced, general-purpose stainless steel. The GP1 powder is nitrogen atomized. Feedstock powder grains are shown in Fig. 1.

$10 \times 10 \times 6$ mm cubic specimens were produced. The specimens were subjected to air as well as ultrasound cleaning and subsequent grinding prior to hardness measurement immediately after manufacture. Seven specimens were made, including a reference specimen. Six of them were heat treated (ST-PH600), either solution treated or solutionized, and aged (age or precipitation hardening). Powder particles were characterised by mostly spherical shapes with some satellites; however, some irregular shape particles were also present. The average size of particles ranged from 40 to 55 µm. Figure 1 shows the fabricated part with its dimensions and with a visible surface texture.

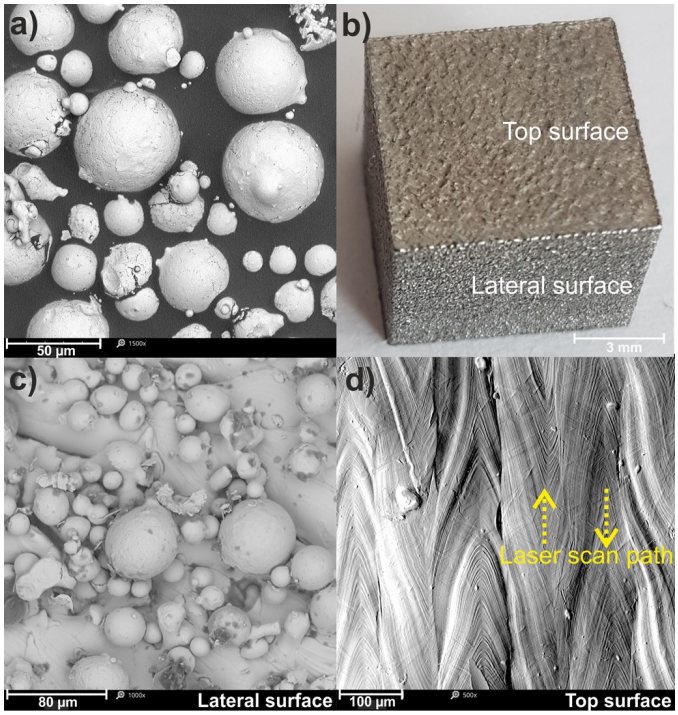


**Fig. 1.** a) Feedstock powder morphology-SEM; b) Printed part; c) Lateral surface-SEM; d) Top surface-SEM

The applied sintering parameters are given in Table 1. The sintering process was carried out on an EOS printer, EOSINT M280.

**Table 1**
Sintering parameters

| Laser power | Laser scanning speed | Layer thickness | Laser spot size | Shielding atmosphere |
|---|---|---|---|---|
| 200 W | 1000 mm/s | 0.02 mm | 0.01 mm | Nitrogen |

The chemical composition, according to the manufacturer, corresponds to the US standards for 17-4PH and 1.4542, AISI 630, and X5CrNiCuNb16-4 steels. The treatment was carried out in an electric chamber furnace, type LAC-LH15. The heat treatment was selected for the steel based on the guidelines found in the EN 10088-3 material standard and in preliminary studies. The solutionizing took place at 1040°C for 40 min. Precipitation hardening was carried out at the temperatures given in Table 2, with the ageing time maintained constant at 240 min and cooling performed in the open air. In Table 2, AP stands for as-printed, ST-solution treatment, PH- precipitation hardening process.

Table 2 shows the load-displacement curves obtained for the nano-test range according to the Oliver-Pharr method. The ma-

terial exhibits an elastic-plastic behaviour. The left-hand side of the curve corresponds to loading, while the right-hand side to unloading. The area under the curve is a plastic work $W_{\text{plast}}$, while that under the curve plot (the area between the extreme point of the plot on the right and the straight line running parallel to the $Y$ axis from that point to the $X$ axis) is an elastic work $W_{\text{elast}}$.

**Table 2**
Sample designation and processing

| Sample designation | Heat treatment | | | |
|---|---|---|---|---|
| | Solution treatment | Time [min] | Age hardening | Time [min] |
| AP (as-printed) | – | – | – | – |
| ST1040 | 1040°C | 40 | – | – |
| PH400 | 1040°C | 40 | 400°C | 240 |
| PH450 | 1040°C | 40 | 450°C | 240 |
| PH500 | 1040°C | 40 | 500°C | 240 |
| PH550 | 1040°C | 40 | 550°C | 240 |
| PH600 | 1040°C | 40 | 600°C | 240 |

The DMLS samples were examined for chemical composition using a Q8 Magellan spark excitation optical emission spectrometer. Three burn-throughs (sparks) were performed for each sample.

Vickers hardness was measured using a Future Tech FM-800 hardness tester with a load of 1.96 N. The samples were ground and well-polished, and the dwell time was set to 15 s. Hardness was measured in the materials raw state, after solution treatment, and after ageing. Nine measurements were taken on each sample at a room temperature of approximately 20°C.

The metallographic samples were ground with 400- and 600-grit papers to remove imprints from the hardness tests. The samples were then flooded with epoxy resin and ground with #600, 800, 1200, 1500, 1800, 2000, and 2200 grit papers. After grinding, they were polished with a 3 µm diamond powder suspension using lubricant. The ground samples were examined under a microscope (Nikon MA200 optical microscope at ×200 magnification) and then etched with a Mi18Fe reagent.

The nanoindentation test was conducted with the Oliver-Pharr method. A Micro Combi Tester (Anton Paar GmbH, Germany) was used to that end. Sixty indentations were made with a V-J 12 Vickers diamond indenter. The test load was increased from the moment the indenter contacted the test surface until the test force $F_{\max}$ was reached at a uniform rate of 800 mN/min. Once $F_{\max}$ was reached, it was held for 10 seconds and then the indenter was unloaded at a uniform rate of 800 mN/min. The force ($F$) and the indenter penetration ($h$) were measured during the test. The test was performed under an $F_{\max}$ load of 300 mN. Hardness and elastic modulus values were calculated from force-displacement data by the Oliver-Pharr method [30]. Parameters such as $E_r$, $E^*$, $HV_{IT}$, $H_{IT}$ were calculated in compliance with ISO 14577-1:2015-09. The following equations (1)–(4) were used for conversion:

$$E_r = \frac{\sqrt{\pi}\cdot S}{2\cdot\beta\sqrt{A_p(h_c)}}, \tag{1}$$

$$E^* = \frac{1}{\frac{1}{E_r} - \frac{1-v_i^2}{E_i}}, \tag{2}$$

$$H_{IT} = \frac{F_{\max}}{A_p}, \tag{3}$$

$$HV_{IT} \approx \frac{H_{IT}}{10.58}, \tag{4}$$

$E_r$ – reduced modulus [Pa],
$E^*$ – plane strain modulus [Pa],
$H_{IT}$ – indentation hardness [Pa],
$HV_{IT}$ – Vickers hardness calculated from $H_{IT}$ [Vickers],
$S$ – contact stiffness N/m,
$\beta$ – geometric factor,
$A_p$ – projected contact area [m$^2$],
$h_c$ – contact depth of the indenter with the sample at $F_{\max}$,
$E_r$ – reduced modulus,
$E_i$ – elastic modulus of the indenter,
$v_i$ – Poisson's ratio.

To compare the obtained results with the previous paper XRD methodology complies with the methodology given in [31]. The phase composition studies were carried out using a Panalytical Empyrean X-ray diffractometer. The filtered X-ray radiation of the CuK$\alpha$1 lamp $\lambda = 0.154051$ nm was used by applying the Bragg-Brentano diffraction geometry. The following parameters were chosen to procure the diffractogram: angle range of diffraction pattern $2\theta = 30$–$100°$, angular step $2\theta = 0.01°$, counting time for one angular step $t = 6$ s and X-ray tube power of 1200 W (40 kV and 30 mA). The phase composition was determined using HighScore Plus v. 3.0e using Crystallography Open Database.

## 3. RESULTS AND DISCUSSION

### 3.1. Chemical composition

The chemical composition analysis showed that the composition complied with the requirements of EN10088-1 and ASTM A564 as well as the manufacturer's specifications. It is worth noting that the chemical composition analysis showed a low sulphur content of 0.005%. Chemical composition results are given in Table 3.

The study demonstrates that the low sulphur content in the 17-4PH steel samples has a positive effect on reducing their corrosion potential. Potentially formed MnS sulphides may become nucleation sites for corrosion pits [32].

The addition of molybdenum increases the passive current density and the critical current density for the passivation of the 17-4PH steel samples. As the amount of molybdenum is increased, the amount of delta ferrite increases, which reduces the hardness of this steel grade [33]. This means that chemical composition is of vital importance for the microstructure and properties of additive-manufactured steel.

**Table 3**
Chemical composition of tested samples

| Element | C | Cr | Ni | Cu | Mn | Si | Mo | Nb | P | S |
|---|---|---|---|---|---|---|---|---|---|---|
| Wt. Powder | 0.01 | 15.8 | 4.02 | 3.9 | 0.7 | 0.7 | 0.4 | 0.29 | – | – |
| Wt. Content as-fabricated % | 0.043 | 15.85 | 4.92 | 4.79 | 0.67 | 0.71 | 0.12 | 0.27 | 0.02 | 0.005 |
| As-fabricated SD | 0.001 | 0.029 | 0.025 | 0.042 | 0.002 | 0.007 | 0.007 | 0.001 | 0.001 | 0.000 |
| EOS powder declaration | $< 0.07$ | 15–17.5 | 3–5 | 3–5 | $< 1$ | $< 1$ | $< 0.5$ | 0.15–0.45 | Bal. | $< 0.07$ |
| EN10088-1 | $< 0.07$ | 15–17 | 3–5 | 3–5 | $< 1.5$ | $< 0.7$ | $< 0.6$ | $5 * C - 0.45$ | $< 0.04$ | 0.03 |
| ASTM A564 | $< 0.07$ | 15–17.5 | 3–5 | 3–5 | $< 1$ | $< 1$ | $< 0.5$ | 0.15–0.45 | – | – |

### 3.2. Microstructure

Figure 2 shows the morphology of test specimens. The untreated 17-4PH steel sample is characterised by an austenitic and martensitic structure. The presence of thick needle-like tempered martensite is a result of solution treatment and ageing processes. The largest grain size was observed for the sample aged at 400°C. Moreover, an analysis of the micrographs reveals the presence of an austenitic phase, as visible in the bright areas. Studies by Ziewiec *et al.* [34] have shown that austenite could also occur at higher ageing temperatures. As the ageing temperature increases, the grain size decreases, and the amount of martensite increases.

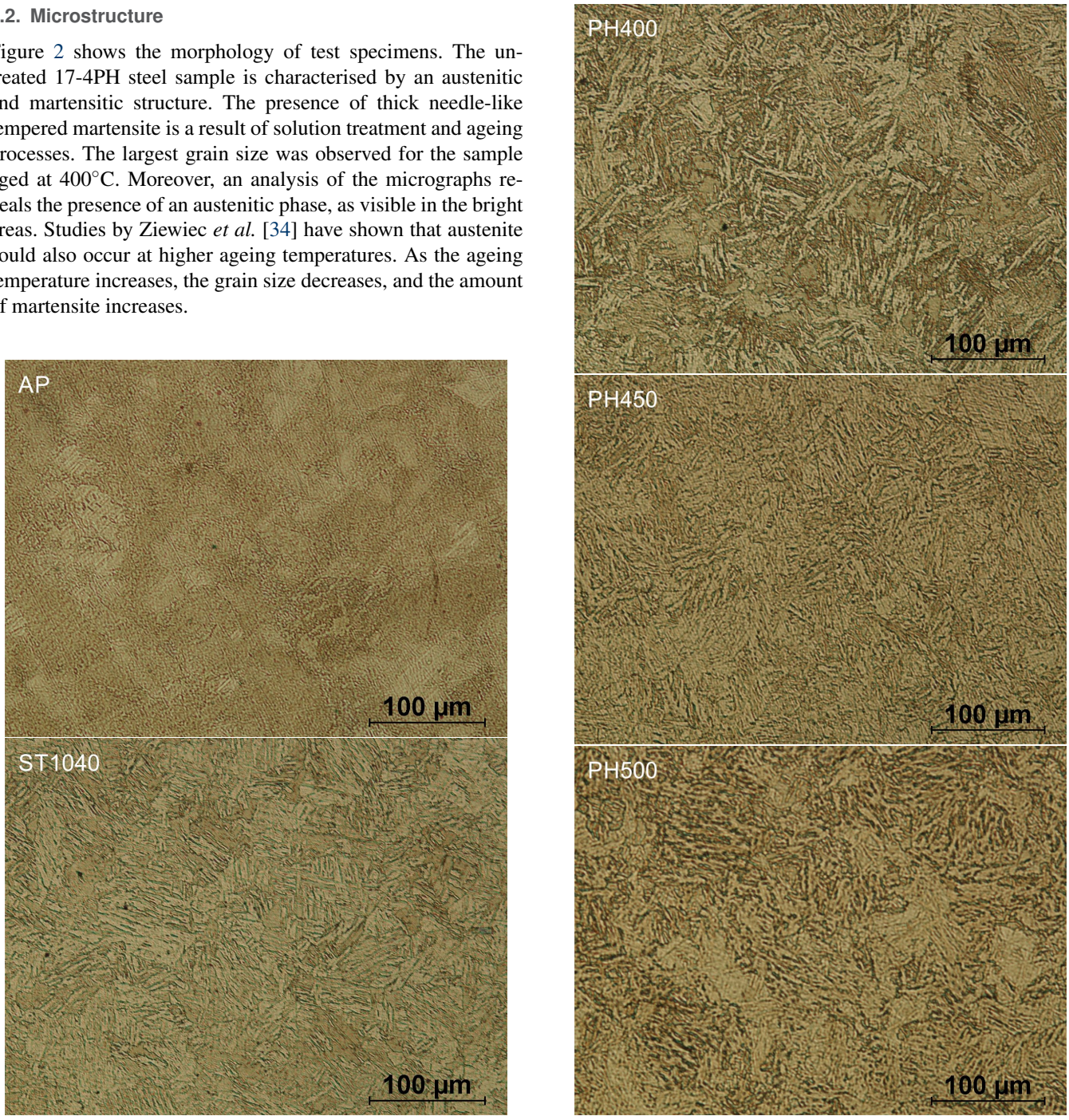

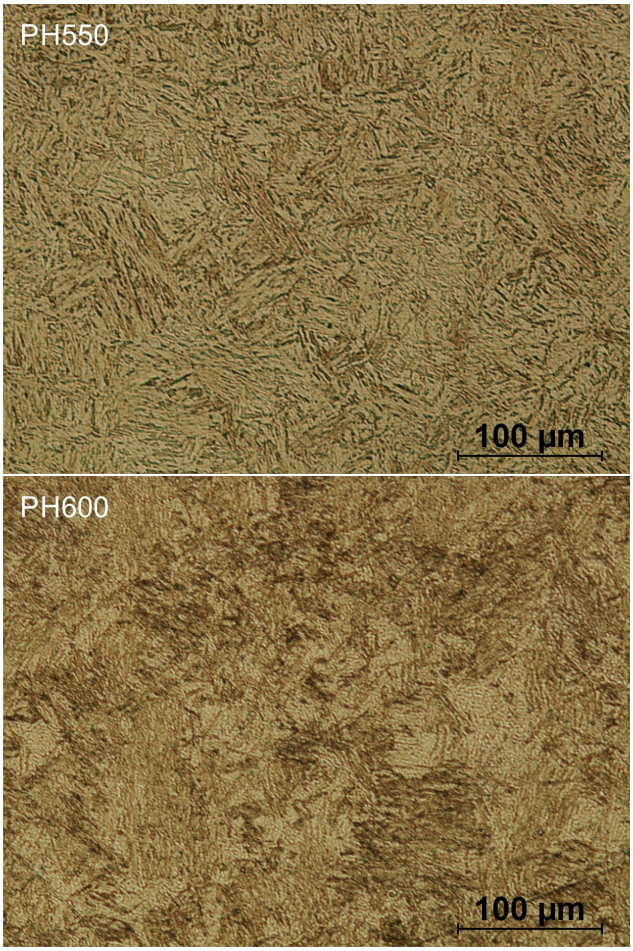


**Fig. 2.** Microstructure of 17-4PH specimens

H. Eskandari *et al.* [35] found that wrought alloy samples had a smaller grain size than as-printed samples. They also observed the presence of a smaller grain size of martensite in the lower part of a sample, which might be related to a lower cooling rate and heat accumulation. Previous studies on the behaviour of 17-4PH steel reported the presence of a martensitic microstructure in this metallic material subjected to solutionizing and cooling down to room temperature [21, 36]. However, due to low hardness, ageing is used, and at temperatures of 480–620°C. A copper-rich phase is formed within the martensitic matrix, which increases hardness and strength [37]. The best results of precipitation hardening may be obtained with ageing in the temperature range of 450–510°C. In this temperature range: coherent copper-rich clusters precipitate, incoherent copper-rich clusters precipitate at temperatures above 540°C, and reversed austenite formation occurs at temperatures around 570°C and above [38]. The formation of reversed austenite may be related to pre-existing copper particles, but there is no clear agreement between these [19, 39]. It has been observed that nitrogen can improve corrosion resistance under neutral pH conditions, among others. The laser powder bed fusion (LPBF) process can produce 17-4PH steel with improved or similar corrosion performance compared to the conventional wrought 17-4PH grade [40].

### 3.3. X-ray diffraction

In order to check the effect of heat treatment on the microstructure and phase composition of AM steel, X-ray diffraction (XRD) measurements were carried out. The measurement results for the untreated and thermally treated samples are shown in Fig. 3. All XRD profiles show the same set of diffraction peaks that differ in relative intensities. Phase analysis was performed with HighScore Plus v. 3.0e using Crystallography Open Database. It was found that the peak positions correspond to both BCC $\alpha$-martensite and FCC $\gamma$-austenite. The phase analysis performed indicates that the diffraction positions of peaks around $2\theta = 44.6$, 64.9, and 82.1 in XRD patterns are in good agreement with the diffraction of peak positions of $\alpha$-martensite (Card No.: COD 96-901-3474). However, the positions of the diffraction peaks at $2\theta = 43.5$, 50.7, and 74.6 in XRD patterns correspond to the peak positions of $\gamma$-austenite (Card No.: COD 96-901-4477). Based on the phase analysis, it can be concluded that all tested samples consist of two phases. Our results are in contrast to the study of Eskandari *et al.* [35] that concluded the austenite in the structure may be retained austenite. Moreover, there was a change in the $\alpha$ and $\gamma$ phase intensity and FWHM (Full Width Half Maximum), which indicated phase transition. The differences in the relative peak heights indicate different proportions of the individual phases. The $\alpha$ phase increased when the $\gamma$-austenite phase decreased in specimens from AP up to PH400 then decreased in the PH450 sample. Then from PH500 up to PH600 amount of martensite increased with the ageing temperature. The applied Rietveld analysis allowed us to determine the proportion of the performed number of individual phases. Percentages of individual phases in individual samples are summarized in Table 4.

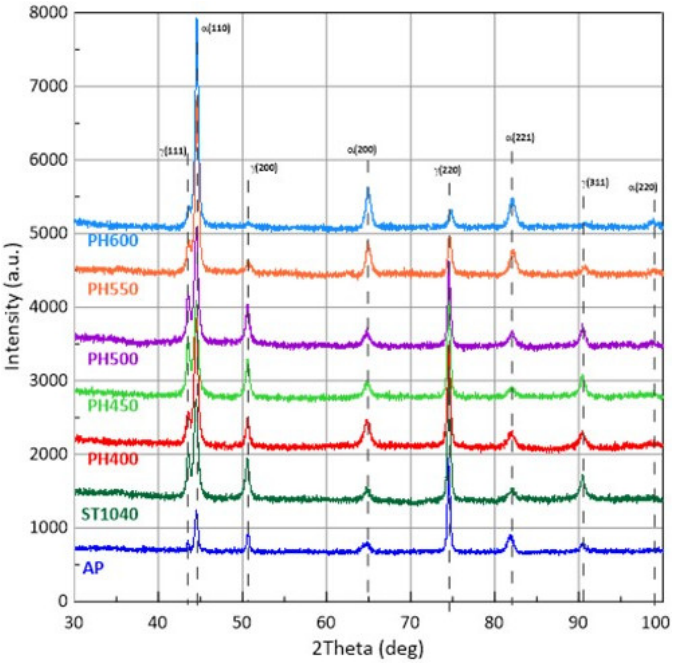


**Fig. 3.** XRD patterns of untreated (AP) and annealed (ST1040, PH400, PH450, PH500, PH550, PH600) 17-4PH stainless steel samples. The annealing temperature is indicated in the sample names

**Table 4**
Percentage of individual phases in samples

| Sample | AP (%) | ST1040 (%) | PH400 (%) | PH450 (%) | PH500 (%) | PH550 (%) | PH600 (%) |
|---|---|---|---|---|---|---|---|
| $\alpha$-martensite | 23 | 49 | 62 | 46 | 53 | 75 | 90 |
| $\gamma$-austenite | 77 | 51 | 38 | 54 | 47 | 25 | 10 |

Looking at the relative heights of the peaks, we can conclude that the grains of the $\alpha$-martensite structure do not show any texture for lower heating temperature and a slight texture for higher heating temperatures in the direction $< 011 >$ perpendicular to the surface of the sample. On the other hand, the height of peak $\gamma$ (220) relative to the other peaks of this phase suggests the arrangement of grains of this phase with planes (220) perpendicular to the surface of the sample. This effect decreases as the heating temperature increases.

A number of studies have found that differences in microstructure may also result from the gas used during fabrication. With the use of nitrogen for fabrication, it is possible to obtain an austenitic-martensitic structure in the case of precipitation-hardening steels with an austenite content of 50–75% and a martensitic content of 25–50%. By using argon, it is possible to obtain a predominantly martensitic structure up to 92% [36, 41, 42]. The gas used for powder atomisation also has a similar effect, i.e. by using nitrogen it is possible to obtain a microstructure with a higher amount of austenite and by using argon it is possible to increase the martensite content. The gas used for atomization also has some effect on the behaviour of the steel in a corrosive environment. However, these are changes that may not occur in a given case because, as previously stated, there are many factors that influence the composition and structure of an additively manufactured material. An example of this can be found in the studies carried out by Murr *et al.* [10] using SLS and argon-atomised powder in a nitrogen environment to obtain a martensitic microstructure. H. Eskandari *et al.* [35] on the other hand obtained austenitic-martensitic structure by using DMLS and the same gases. It was observed that nitrogen can improve corrosion resistance under neutral pH conditions. The Laser Powder Bed Fusion (LPBF) process can produce 17-4PH steel with better or similar corrosion performance compared to conventional wrought 17-4PH [40]. In summary, gas used in the fabrication and atomization of powder as well as the temperature of ageing process strongly affects the final structure and properties.

After ageing, it is noticeable that martensitic crystallite size increase with the rising ageing temperature from 450°C to 600°C, and that is a general trend for this phase. Figure 4 shows the evolution of crystallite size determined from the peaks diffraction positioned around the $2\theta = 44$, 62, and 82 degrees. Immediately after fabrication, the largest martensitic crystallite size was obtained, then the size decreased in PH450 and PH500. This phenomenon may be associated with Cu precipitation in the martensitic matrix, which occurs under similar conditions of temperature and heating time [43]. PH600 specimen had the largest martensitic crystallite size after ageing and the lowest hardness and PH450 specimen has the smallest crystallite size and highest hardness. The difference in the evolution of crystallite sizes obtained for different peaks may be due to the height of individual peaks and the related precision of FWHM determination and separation of part of the peaks broadening caused by the size of the crystallites.

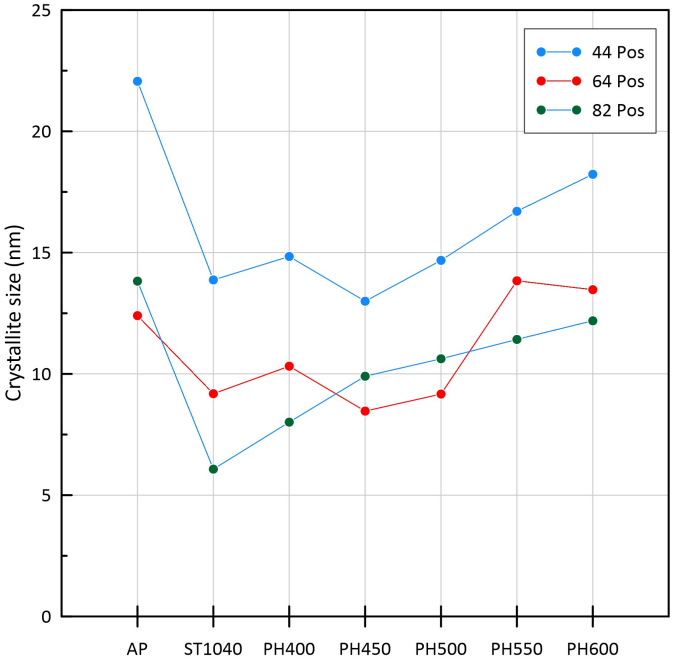


**Fig. 4.** Crystallite size in nm for $\alpha$ martensitic determined based on FWHM of peaks at around $2\theta = 44°$ (110), 64° (200), 82° (211)

### 3.4. Hardness measurements

Vickers hardness results are given in Table 5. The highest increase in hardness after precipitation hardening amounting to 77% was obtained for the PH450 specimen that was hardened at 450°C. The lowest hardness was obtained for the as-fabricated sample (AP). The lowest increase in hardness of 15% was obtained with precipitation hardening at 600°C. The hardness after manufacture was $216 \pm 11.9$ $HV_{0.2}$, even though the man-

**Table 5**
Comparison of $HV_{0.2}$ hardness parameter

| Sample | AP | ST1040 | PH400 | PH450 | PH500 | PH550 | PH600 |
|---|---|---|---|---|---|---|---|
| Mean | 216 | 309 | 344 | 382 | 334 | 360 | 248 |
| SD | 11.9 | 10.1 | 16.4 | 10.3 | 17.7 | 17.7 | 14.8 |

ufacturer of the powder gives $230 \pm 20$ $HV_{0.2}$ as the nominal value.

The hardness values after manufacture without heat treatment are similar to those obtained by Etemadi *et al*. for alloy 17-4PH produced by casting after solution treatment, and they are below 20 HRC, which corresponds to 227 HV. After cold treatment the hardness was 30-40 HRC and after ageing 23–47 HRC and 40–45 HRC, which corresponded to 285–474 HV and 388–448 HV [44]. After precipitation hardening Bressan *et al.* [37] obtained the hardness of 33 HRC, 37 HRC, and 43 HRC, which corresponded to 311 HV, 351 HV, and 424 HV, respectively. Gratton *et al.* [45] obtained 258 HV in a raw state, 221 $HV_{20}$ after solution treatment, and 225 $HV_{20}$ in the H900 condition. On the other hand, Guennouni *et al*. [25] obtained 330–349 $HV_{0.1}$ in the as-printed condition and 344–353 $HV_{0.1}$ in the H900 condition. The conventionally fabricated part in H900 had a hardness of 371 $HV_{0.1}$ and 387 $HV_{0.1}$ in H1025. Compared to other studies [36, 46, 47], the specimens had different hardness values after solution treatment and after ageing. This may be due to differences in time and slight differences in temperature; this may also result from the applied type of hardening, as most studies use the conditions from H900 to H1150 that utilize water quenching rather than air quenching (which was the case in this study). These differences may also be due to differences in gas. 17-4PH materials fabricated in a nitrogen atmosphere are usually harder than those made with argon due to the greater martensite to austenite ratio.

### 3.5. Nanoindentation – mechanical properties

Nanoindentation results obtained for the test specimens are given in Table 6.

An analysis of the nanoindentation results demonstrates that PH450 has the highest hardness (5.89 GPa). The lowest hardness of 3.33 GPa is obtained for ST1040. The highest modulus of elasticity is obtained for PH500 (198.49 GPa) and the lowest for ST1040 (198.49 GPa). PH450 also exhibits the highest value of the $H/E$ parameter, which implies the highest wear resistance of this material [48]. The nanoindentation results were then analysed for their correlation with the Vickers hardness results obtained with the micro indenter, and the Shapiro-Wilk test showed that the variables had a normal distribution. This indicates that the global hardness agrees with the local hardness (Fig. 5). For all examined cases, the percentage of plastic and elastic work to the total work is the same. The elastic work amounts to 14.53%, while the plastic work is 86.59%.

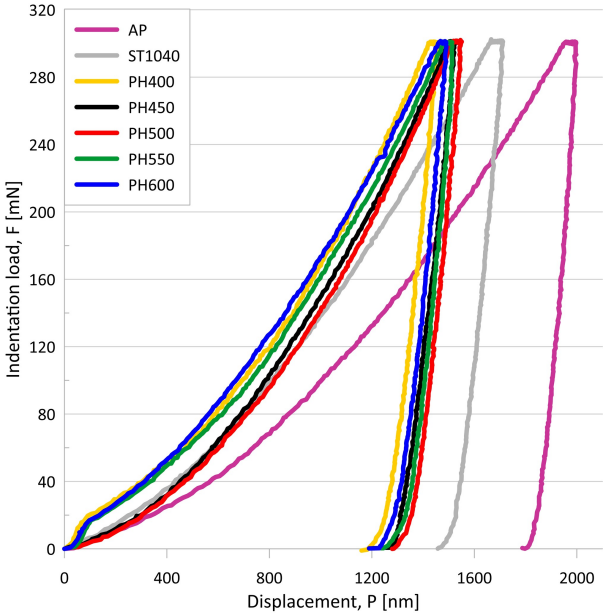


**Fig. 5.** Load versus displacement nanoindentation curves

The H/E ratio is particularly important in terms of erosive wear resistance, as it facilitates the estimation of a given material resistance to this type of wear [49]. On the other hand, $H^2/E^2$ is a strong indicator of material resistance to plastic deformation. Erosive wear causes many operational problems, particularly cavitation erosion [50]. Although it is an extremely intense and degrading phenomenon, cavitation may be utilized for cavitation peening [51]. Due to the high intensity of a single pulse, the layer can be strengthened relatively deep below the surface. Another important advantage of additively manu-

**Table 6**

Nanoindentation results, $H_{IT}$ – hardness, $E$ – elastic modulus, $W_{elast}$ – elastic work, $W_{plast}$ – plastic work, $W_{total}$ – total work

| Parameter | AP | ST1040 | PH400 | PH450 | PH500 | PH550 | PH600 |
|---|---|---|---|---|---|---|---|
| $H_{IT}$ [GPa] | 4.33 | 3.33 | 5.62 | 5.89 | 5.40 | 5.61 | 5.58 |
| $SD_H$ | 0.53 | 0.53 | 0.50 | 1.28 | 0.95 | 0.97 | 0.65 |
| $E$ [GPa] | 207.42 | 198.49 | 221.25 | 223.41 | 252.77 | 223.31 | 242.62 |
| $SD_E$ | 14 | 26 | 17 | 19 | 20 | 28 | 24 |
| $H/E$ | 0.016769 | 0.016769 | 0.025407 | 0.026367 | 0.021355 | 0.025144 | 0.023008 |
| $H^2/E^2$ | 0.000936 | 0.000936 | 0.003629 | 0.004095 | 0.002462 | 0.00355 | 0.002955 |
| $W_{elast}$ [μJ] | 0.027857 | 0.028788 | 0.02898 | 0.0285 | 0.028421 | 0.028413 | 0.02873 |
| $W_{plast}$ [μJ] | 0.166071 | 0.160758 | 0.165306 | 0.160667 | 0.165263 | 0.164444 | 0.164444 |
| $W_{total}$ [μJ] | 0.191786 | 0.187273 | 0.191633 | 0.190167 | 0.191579 | 0.191111 | 0.191111 |

factured materials is the possibility of using peening in regions inaccessible to other peening methods. Tribological parameters can be tailored to a specified environment by appropriate heat treatment, changing matrix morphology and size, as well as due to the presence of hard phases [52].

Results of Vickers hardness and indentation hardness according to the Oliver-Pharr method obtained for different temperatures are given in Fig. 6.

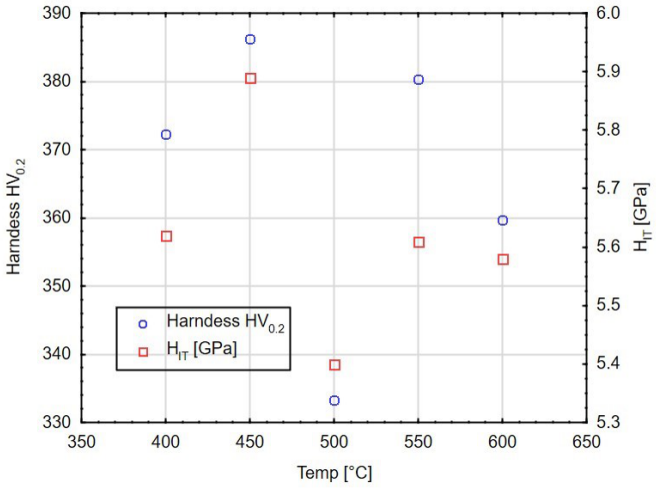


**Fig. 6.** Hardness versus precipitation hardening temperature

Figure 6 shows the relationship between ageing temperature (the solution treatment temperature was maintained constant) and hardness. It can be observed that the highest hardness is obtained at temperatures ranging between 450 and 490°C [28]. Other studies [19,53] have also reported this temperature range to be the most suitable for the 17-4PH grade of steel due to the precipitation of Cu and Nb phases and the MS temperature of approx. 480°C.

## 4. CONCLUSIONS

The work explores the effects of heat treatment conditions in particular ageing temperatures on microstructure and mechanical properties. Based on the research, the following conclusions can be drawn:

- The microstructural examination results confirmed that the obtained structure was typical of additive-manufactured 17-4PH steel, as it contained a fine-grained needle-like structure. A two-phase structure with fine martensite needles, consisting of austenite and martensite, was observed in the as-built state. The top and inner surfaces showed overlapping laser beam pass patterns.
- XRD measurements suggest that when 17-4PH steel is heated, the transition of the austenite phase to martensite takes place, accompanied by the disappearance of the texture of the austenite crystallites. It was observed that the size of crystallites was refined from 12.5–22 nm to 7–14 nm in the structure after solution treatment at temp 1040°C. The martensite crystallite size generally increased with ageing temperature, except for the PH450 specimen.
- Heat treatment had positive effects on the properties of 17-4PH steel, Vickers hardness by 15–77%, elastic modulus by 7–22%, resistance to plastic deformation ($H^2/E^2$) 215–337%, and resistance to abrasive wear ($H/E$) 27–57%. The highest hardness of 382 $HV_{0.2}$ was obtained for the PH450 sample that was precipitation hardened at 450°C. The lowest hardness (216 $HV_{0.2}$) was observed for AP in as-fabricated condition; a low hardness of 248 $HV_{0.2}$ was also obtained for the samples subjected to precipitation hardening with ageing at 600°C. The lowest $H/E$ ratio of 0.000936 was obtained for the samples subjected to printing and solution treatment. The highest $H/E$ ratio of 0.026367 was observed for the PH450 sample.
- The increase in the ageing temperature did not directly affect the change in the analysed properties in a specific direction except for the size of the crystallites and the content of the different phases.
- Moreover, the results showed a general relationship between hardness and grain size. The PH450 sample had the highest hardness but a small grain size. ST1040, on the other hand, exhibited the lowest hardness after solution treatment. The samples PH400, PH500, and PH600 had a relatively coarse grain size and low hardness.
- PH400 and PH550 samples had similar properties and the differences in hardness can be explained by the 13% higher martensite content in the PH550 sample.
- The best conditions for the ageing process were at 450°C. Sample PH450 had the best properties in practically all the tests carried out, slightly better elastic properties were characteristic of sample PH500.
- With constant solution treatment conditions, the selection of an appropriate ageing temperature seems to be crucial for obtaining the desired properties. Interestingly, after the solution treatment process, an equal ratio of austenite to martensite content was obtained, and temperature modification resulted in a change in austenite content to the range of 10% to 54%. Martensite as a hard phase, however, does not seem to be responsible for the overall increase in hardness after the ageing process, although the noted reduction in crystallite size in the PH450 sample is a beneficial effect. Thus, it is possible that this is due to the strengthening resulting from the formation of carbides or the formation of precipitates at grain boundaries.

## ACKNOWLEDGEMENTS

The project was financed by Union of Lublin Universities as part of the programme “INTERPROJECT” (Grant nr: INT/005/2022/I-N).

## REFERENCES

[1] A. Ziewiec, A. Zielińska-Lipiec, and E. Tasak, “Microstructure of Welded Joints of X5CrNiCuNb16-4 (17-4 PH) Martensitic Stainlees Steel After Heat Treatment,” *Arch. Metall. Mater.*, vol. 59, no. 3, pp. 965–970, Oct. 2014, doi: 10.2478/amm-2014-0162.

[2] M. del R. Lara Banda, D.Y. Pérez Ortíz, C. Gaona Tiburcio, P. Zambrano-Robledo, J.A. Cabral Miramontes, and F. Almeraya Calderon, "Citric Acid Passivation of 15-5PH and 17-4PH Stainless Steel Used in the Aeronautical Industry," in *Proc. of the Symposium of Aeronautical and Aerospace Processes, Materials and Industrial Applications*, P. Zambrano-Robledo, A. Salinas-Rodriguez, and F. Almeraya Calderon, Eds., Cham: Springer International Publishing, 2018, pp. 95–104. doi: 10.1007/978-3-319-65611-3_9.

[3] B. Alım *et al.*, "Precipitation-hardening stainless steels: Potential use radiation shielding materials," *Radiat. Phys. Chem.*, vol. 194, p. 110009, May 2022, doi: 10.1016/j.radphyschem.2022.110009.

[4] M. Yousefi, M. Rajabi, M. Yousefi, and M.S. Amiri Kerahroodi, "Failure Analysis of a 17-4PH Stainless Steel Part in an Exhaust Fastener," *J. Fail. Anal. Preven.*, vol. 21, no. 6, pp. 2278–2289, Dec. 2021, doi: 10.1007/s11668-021-01291-8.

[5] F.J. Alamos *et al.*, "Effect of powder reuse on orthopedic metals produced through selective laser sintering," *Manuf. Lett.*, p. S2213846321000407, Jun. 2021, doi: 10.1016/j.mfglet.2021.06.002.

[6] D.Y. Park *et al.*, "Development of hydrophobic surgical forceps using powder injection molding and surface treatment," *Arch. Metall. Mater.*, vol. 63, no. 1, Mar. 2018, doi: 10.24425/118964.

[7] Y. Bozkurt and E. Karayel, "3D printing technology; methods, biomedical applications, future opportunities and trends," *J. Mater. Res. Technol-JMRT*, vol. 14, pp. 1430–1450, Sep. 2021, doi: 10.1016/j.jmrt.2021.07.050.

[8] S. Cooke, K. Ahmadi, S. Willerth, and R. Herring, "Metal additive manufacturing: Technology, metallurgy and modelling," *J. Manuf. Process.*, vol. 57, pp. 978–1003, Sep. 2020, doi: 10.1016/j.jmapro.2020.07.025.

[9] Kh. Moeinfar, F. Khodabakhshi, S.F. Kashani-bozorg, M. Mohammadi, and A.P. Gerlich, "A review on metallurgical aspects of laser additive manufacturing (LAM): Stainless steels, nickel superalloys, and titanium alloys," *J. Mater. Res. Technol-JMRT*, vol. 16, pp. 1029–1068, Jan. 2022, doi: 10.1016/j.jmrt.2021.12.039.

[10] L.E. Murr *et al.*, "Microstructures and Properties of 17-4 PH Stainless Steel Fabricated by Selective Laser Melting," *J. Mater. Res. Technol-JMRT*, vol. 1, no. 3, pp. 167–177, Oct. 2012, doi: 10.1016/S2238-7854(12)70029-7.

[11] D. Ding, Z. Pan, D. Cuiuri, and H. Li, "Wire-feed additive manufacturing of metal components: technologies, developments and future interests," *Int. J. Adv. Manuf. Technol.*, vol. 81, no. 1–4, pp. 465–481, Oct. 2015, doi: 10.1007/s00170-015-7077-3.

[12] W. Macek, R.F. Martins, R. Branco, Z. Marciniak, M. Szala, and S. Wroński, "Fatigue fracture morphology of AISI H13 steel obtained by additive manufacturing," *Int. J. Fract.*, Jan. 2022, doi: 10.1007/s10704-022-00615-5.

[13] H.R. Lashgari, Y. Xue, C. Onggowarsito, C. Kong, and S. Li, "Microstructure, Tribological Properties and Corrosion Behaviour of Additively Manufactured 17-4PH Stainless Steel: Effects of Scanning Pattern, Build Orientation, and Single vs. Double scan," *Mater. Today Commun.*, vol. 25, p. 101535, Dec. 2020, doi: 10.1016/j.mtcomm.2020.101535.

[14] M. Walczak and M. Szala, "Effect of shot peening on the surface properties, corrosion and wear performance of 17-4PH steel produced by DMLS additive manufacturing," *Archiv. Civ. Mech. Eng.*, vol. 21, no. 4, p. 157, Dec. 2021, doi: 10.1007/s43452-021-00306-3.

[15] Y. Zhang and J. Zhang, "Finite element simulation and experimental validation of distortion and cracking failure phenomena in direct metal laser sintering fabricated component," *Addit. Manuf.*, vol. 16, pp. 49–57, Aug. 2017, doi: 10.1016/j.addma.2017.05.002.

[16] M. Shehata, T.M. Hatem, and W.A. Samad, "Experimental Study of Build Orientation in Direct Metal Laser Sintering of 17-4PH Stainless Steel," *3D Print. Addit. Manuf.*, vol. 6, no. 4, pp. 227–233, Aug. 2019, doi: 10.1089/3dp.2017.0106.

[17] G. Yeli, M.A. Auger, K. Wilford, G.D.W. Smith, P.A.J. Bagot, and M.P. Moody, "Sequential nucleation of phases in a 17-4PH steel: Microstructural characterisation and mechanical properties," *Acta Mater.*, vol. 125, pp. 38–49, Feb. 2017, doi: 10.1016/j.actamat.2016.11.052.

[18] J. Sripada *et al.*, "Effect of hot isostatic pressing on microstructural and micromechanical properties of additively manufactured 17–4PH steel," *Mater. Charact.*, vol. 192, p. 112174, Oct. 2022, doi: 10.1016/j.matchar.2022.112174.

[19] C.N. Hsiao, C.S. Chiou, and J.R. Yang, "Ageing reactions in a 17-4 PH stainless steel," *Mater. Chem. Phys.*, vol. 74, no. 2, pp. 134–142, Mar. 2002, doi: 10.1016/S0254-0584(01)00460-6.

[20] J. Tian, W. Wang, W. Yan, Z. Jiang, Y. Shan, and K. Yang, "Cracking due to Cu and Ni segregation in a 17-4 PH stainless steel piston rod," *Eng. Fail. Anal.*, vol. 65, pp. 57–64, Jul. 2016, doi: 10.1016/j.engfailanal.2016.03.011.

[21] S. Cheruvathur, E.A. Lass, and C.E. Campbell, "Additive Manufacturing of 17-4 PH Stainless Steel: Post-processing Heat Treatment to Achieve Uniform Reproducible Microstructure," *JOM-J. Miner. Met. Mater. Soc.*, vol. 68, no. 3, pp. 930–942, Mar. 2016, doi: 10.1007/s11837-015-1754-4.

[22] I. Mutlu and E. Oktay, "Characterization of 17-4 PH stainless steel foam for biomedical applications in simulated body fluid and artificial saliva environments," *Mater. Sci. Eng.-C*, vol. 33, no. 3, pp. 1125–1131, Apr. 2013, doi: 10.1016/j.msec.2012.12.004.

[23] R. Singh, J.S. Sidhu, Rishab, B.S. Pabla, and A. Kumar, "Three-Dimensional Printing of Innovative Intramedullary Pin Profiles with Direct Metal Laser Sintering," *J. Mater. Eng. Perform.*, vol. 31, no. 1, pp. 240–253, Jan. 2022, doi: 10.1007/s11665-021-06176-3.

[24] D. Manfredi, F. Calignano, M. Krishnan, R. Canali, E. Ambrosio, and E. Atzeni, "From Powders to Dense Metal Parts: Characterization of a Commercial AlSiMg Alloy Processed through Direct Metal Laser Sintering," *Materials*, vol. 6, no. 3, pp. 856–869, Mar. 2013, doi: 10.3390/ma6030856.

[25] N. Guennouni *et al.*, "Comparative study of the microstructure between a laser beam melted 17-4PH stainless steel and its conventional counterpart," *Mater. Sci. Eng.-A*, vol. 823, p. 141718, Aug. 2021, doi: 10.1016/j.msea.2021.141718.

[26] S.F. Siddiqui, A.A. Fasoro, C. Cole, and A.P. Gordon, "Mechanical Characterization and Modeling of Direct Metal Laser Sintered Stainless Steel GP1," *J. Eng. Mater. Technol.*, vol. 141, no. 3, p. 031009, Jul. 2019, doi: 10.1115/1.4042867.

[27] A.I. Gorunov, O.V. Kudimov, and A.Kh. Gilmutdinov, "Effect of stress concentrators on fracture resistance of specimens fabricated by direct metal laser sintering," *Eng. Fail. Anal.*, vol. 131, p. 105900, Jan. 2022, doi: 10.1016/j.engfailanal.2021.105900.

[28] S.A. Razavi, F. Ashrafizadeh, and S. Fooladi, "Prediction of age hardening parameters for 17-4PH stainless steel by artificial neural network and genetic algorithm," *Mater. Sci. Eng.-A*, vol. 675, pp. 147–152, Oct. 2016, doi: 10.1016/j.msea.2016.08.049.

[29] L. Klimek, E. Wołowiec, and B. Majkowska, "Types of wear and tear of biomaterials used in orthopaedic surgery," *J. Achiev. Mater. Manuf. Eng.*, vol. 56, no. 2, pp. 83–89, 2013.

[30] W.C. Oliver and G.M. Pharr, "Measurement of hardness and elastic modulus by instrumented indentation: Advances in understanding and refinements to methodology," *J. Mater. Res.*, vol. 19, no. 1, pp. 3–20, Jan. 2004, doi: 10.1557/jmr.2004.19.1.3.

[31] M. Szala, M. Walczak, L. Łatka, K. Gancarczyk, and D. Özkan, "Cavitation Erosion and Sliding Wear of MCrAlY and NiCrMo Coatings Deposited by HVOF Thermal Spraying," *Adv. Mater. Sci.*, vol. 20, no. 2, pp. 26–38, Jun. 2020, doi: 10.2478/adms-2020-0008.

[32] S.S. M. Tavares, J.M. Pardal, T.R.B. Martins, and M.R. da Silva, "Influence of Sulfur Content on the Corrosion Resistance of 17-4PH Stainless Steel," *J. Mater. Eng. Perform.*, vol. 26, no. 6, pp. 2512–2519, Jun. 2017, doi: 10.1007/s11665-017-2693-8.

[33] M. Karaminezhaad, S. Sharafi, and K. Dalili, "Effect of molybdenum on SCC of 17-4PH stainless steel under different ageing conditions in chloride solutions," *J. Mater. Sci.*, vol. 41, no. 11, pp. 3329–3333, Jun. 2006, doi: 10.1007/s10853-005-5416-8.

[34] A. Ziewiec, A. Zielińska-Lipiec, J. Kowalska, and K. Ziewiec, "Microstructure Characterization of Welds in X5CrNiCuNb16-4 Steel in Overaged Condition," *Adv. Mater. Sci.*, vol. 19, no. 1, pp. 57–69, Mar. 2019, doi: 10.2478/adms-2019-0005.

[35] H. Eskandari, H.R. Lashgari, L. Ye, M. Eizadjou, and H. Wang, "Microstructural characterization and mechanical properties of additively manufactured 17–4PH stainless steel," *Mater. Today Commun.*, vol. 30, p. 103075, Mar. 2022, doi: 10.1016/j.mtcomm.2021.103075.

[36] T. LeBrun, T. Nakamoto, K. Horikawa, and H. Kobayashi, "Effect of retained austenite on subsequent thermal processing and resultant mechanical properties of selective laser melted 17–4 PH stainless steel," *Mater. Des.*, vol. 81, pp. 44–53, Sep. 2015, doi: 10.1016/j.matdes.2015.05.026.

[37] J.D. Bressan, D.P. Daros, A. Sokolowski, R.A. Mesquita, and C.A. Barbosa, "Influence of hardness on the wear resistance of 17-4 PH stainless steel evaluated by the pin-on-disc testing," *J. Mater. Process. Technol.*, vol. 205, no. 1–3, pp. 353–359, Aug. 2008, doi: 10.1016/j.jmatprotec.2007.11.251.

[38] B. Rivolta and R. Gerosa, "On the non-isothermal precipitation of copper-rich phase in 17-4 PH stainless steel using dilatometric techniques," *J. Therm. Anal. Calorim.*, vol. 102, no. 3, pp. 857–862, Dec. 2010, doi: 10.1007/s10973-010-0882-x.

[39] B. AlMangour and J.-M. Yang, "Improving the surface quality and mechanical properties by shot-peening of 17-4 stainless steel fabricated by additive manufacturing," *Mater. Des.*, vol. 110, pp. 914–924, Nov. 2016, doi: 10.1016/j.matdes.2016.08.037.

[40] M.R. Stoudt, C.E. Campbell, and R.E. Ricker, "Examining the Relationship Between Post-Build Microstructure and the Corrosion Resistance of Additively Manufactured 17-4PH Stainless Steel," *Materialia*, vol. 22, p. 101435, May 2022, doi: 10.1016/j.mtla.2022.101435.

[41] T. DebRoy *et al.*, "Additive manufacturing of metallic components – Process, structure and properties," *Prog. Mater. Sci.*, vol. 92, pp. 112–224, Mar. 2018, doi: 10.1016/j.pmatsci.2017.10.001.

[42] H.K. Rafi, D. Pal, N. Patil, T.L. Starr, and B.E. Stucker, "Microstructure and Mechanical Behavior of 17-4 Precipitation Hardenable Steel Processed by Selective Laser Melting," *J. Mater. Eng. Perform.*, vol. 23, no. 12, pp. 4421–4428, Dec. 2014, doi: 10.1007/s11665-014-1226-y.

[43] C. Rowolt, B. Milkereit, A. Springer, C. Kreyenschulte, and O. Kessler, "Dissolution and precipitation of copper-rich phases during heating and cooling of precipitation-hardening steel X5CrNiCuNb16-4 (17-4 PH)," *J. Mater. Sci.*, vol. 55, no. 27, pp. 13244–13257, Sep. 2020, doi: 10.1007/s10853-020-04880-4.

[44] A.R. Etemadi, P. Behjati, A. Emami, S.M.-D. Motiei, and S. Mirsaeedi, "Failure analysis of holding yokes made of investment cast 17-4 PH stainless steel," *Eng. Fail. Anal.*, vol. 18, no. 4, pp. 1242–1246, Jun. 2011, doi: 10.1016/j.engfailanal.2011.03.008.

[45] A. Gratton, "Comparison of Mechanical, Metallurgical Properties of 17-4PH Stainless Steel between Direct Metal Laser Sintering (DMLS) and Traditional Manufacturing Methods," *Proceedings of The National Conference On Undergraduate Research (NCUR)*, 2012.

[46] Y. Sun, R.J. Hebert, and M. Aindow, "Effect of heat treatments on microstructural evolution of additively manufactured and wrought 17-4PH stainless steel," *Mater. Des.*, vol. 156, pp. 429–440, Oct. 2018, doi: 10.1016/j.matdes.2018.07.015.

[47] F.R. Andreacola, I. Capasso, L. Pilotti, and G. Brando, "Influence of 3d-printing parameters on the mechanical properties of 17-4PH stainless steel produced through Selective Laser Melting," *Frattura ed Integritŕ Strutturale*, vol. 15, no. 58, pp. 282–295, Sep. 2021, doi: 10.3221/IGF-ESIS.58.21.

[48] M. Szala, M. Walczak, K. Pasierbiewicz, and M. Kamiński, "Cavitation Erosion and Sliding Wear Mechanisms of AlTiN and TiAlN Films Deposited on Stainless Steel Substrate," *Coatings*, vol. 9, no. 5, p. 340, May 2019, doi: 10.3390/coatings9050340.

[49] M. Walczak, K. Pasierbiewicz, and M. Szala, "Adhesion and Mechanical Properties of TiAlN and AlTiN Magnetron Sputtered Coatings Deposited on the DMSL Titanium Alloy Substrate," *Acta Phys. Pol. A*, vol. 136, no. 2, pp. 294–298, Aug. 2019, doi: 10.12693/APhysPolA.136.294.

[50] M. Dojčinović, "Comparative cavitation erosion test on steels produced by ESR and AOD refining," *Mater. Sci.-Pol.*, vol. 29, no. 3, pp. 216–222, Sep. 2011, doi: 10.2478/s13536-011-0034-4.

[51] H. Soyama, "Cavitation Peening: A Review," *Metals*, vol. 10, no. 2, p. 270, Feb. 2020, doi: 10.3390/met10020270.

[52] P.K. Farayibi, J. Hankel, F. van gen Hassend, M. Blüm, S. Weber, and A. Röttger, "Tribological characteristics of sintered martensitic stainless steels by nano-scratch and nanoindentation tests," *Wear*, vol. 512–513, p. 204547, Jan. 2023, doi: 10.1016/j.wear.2022.204547.

[53] Z. Zhao *et al.*, "Effect of Solution Temperature on the Microstructure and Properties of 17-4PH High-Strength Steel Samples Formed by Selective Laser Melting," *Metals*, vol. 12, no. 3, p. 425, Feb. 2022, doi: 10.3390/met12030425.